Self-doping in boron sheets from first principles: A route to structural design of metal boride nanostructures

Hui Tang and Sohrab Ismail-Beigi
Department of Applied Physics, Yale University, New Haven, Connecticut 06520, USA
(Received 19 May 2009; revised manuscript received 1 September 2009; published 15 October 2009)

Based on first-principles methods, we present a self-doping picture in atomically thin boron sheets: this shows that for two-dimensional boron nanostructures, adding or removing boron atoms is essentially equivalent to simply adding or removing electrons from a fixed electronic structure. This picture allows us to propose a general design rule for pure boron nanostructures and explains the occurrence of known stable nanostructures. In addition, self-doping provides a powerful tool for finding stable metal boride nanostructures. We illustrate this last point by showing an unexpectedly stable MgB_2 sheet structure which is likely the precursor of MgB_2 nanotubes. Our results are easily generalized to other stoichiometries and other choices of metals.

DOI: 10.1103/PhysRevB.80.134113 PACS number(s): 61.46.−w, 62.23.−c, 68.65.−k, 73.22.−f

I. INTRODUCTION

Boron is a peculiar element with extremely versatile chemistry. In particular, nanostructures of pure boron have attracted significant attention due to the successful fabrication of pure boron nanotubes in experiments.[1,2] Boron nanotubes were first predicted based on the existence of two-dimensional (2D) quasiplanar boron clusters verified with theory and in experiments.[3–11] All boron nanotubes were predicted to be metallic based on a 2D buckled triangular sheet.[12–15] Recently, a class of 2D boron sheets have been discovered.[16,17] These boron sheets are always metallic and made of mixtures of triangular and hexagonal motifs. The most stable such sheet, denoted as the "α" sheet, has the right ratio of hexagonal and triangular regions for optimal stability. In spite of the fact that the α sheet is metallic, small-radius boron nanotubes made from the α sheet are semiconducting due to the buckling of nanotube surfaces under curvature.[17,18] Furthermore, predictions of stable boron fullerenes,[19–22] which share the α sheet as precursors with boron nanotubes, have made this research field as appealing as carbon nanostructures.

Besides pure boron nanostructures, some earlier works predicted that stable metal boride nanotubes can exist in the form of isolated nanotubes and are further stabilized by forming nanotube bundles.[23–25] These metal boride (MgB_2, AlB_2, and BeB_2) nanotubes were shown to be very good one-dimensional conducting systems and might possibly be superconducting. In fact, the possibility of superconductivity in nanostructures has always been a fascinating subject in physics and materials science. For example, small-radius carbon nanotubes have been shown to be superconducting at low temperatures.[26,27] Beyond carbon-based materials, MgB_2 as a bulk crystal has attracted interest due to the discovery of superconductivity near 40 K.[28] As nanomaterials, researchers have proposed that MgB_2 nanotubes, which could be fabricated by doping boron nanotubes with Mg,[29] may have higher superconducting temperatures than MgB_2 bulk due to electron confinement.[23,30] As a result, MgB_2 nanotubes built from a 2D sheet derived from the bulk structure have been extensively studied in theory.[23,29–32] Besides MgB_2, other metal boride nanotubes are also shown to be intriguing materials. Amorphous metal (Ni, Fe, and Co) boride nanotubes with good catalytic properties are made experimentally.[33,34] Nanostructures of transition-metal borides are shown to be good one-dimensional conductors and promising candidates for hydrogen storage.[35–37] In all, metal boride nanomaterials may prove to be an interesting, versatile, and useful class of materials.

Despite of these fascinating discoveries on metal boride nanomaterials, researchers have not yet successfully addressed a fundamental problem. In all previous analyses, the fundamental 2D sheet giving rise to those metal boride nanostructures is extracted directly from bulk MgB_2. While a reasonable guess, there is no reason *a priori* why this should be the optimal structure. More generally, the proper stoichiometry is not necessarily that of the bulk either: i.e., it is not clear that MgB_x with $x=2$ is the optimal choice for nanostructures. Of course, screening all possible candidate structures with all possible stoichiometries is formidable and hopeless. In this paper, we provide theoretical tools and understanding to organize and accelerate this task. We describe a self-doping picture in boron nanostructures, derived from analyzing the chemical bonding and electron count in boron sheets, that allows us to propose a general design rule for stable boron nanostructures. When applied to 2D metal boride sheets, self-doping narrows down vastly the phase space of possible structures to be considered. As an example, we predict and verify from first principles that the lowest-energy structure of 2D atomically thin MgB_2 sheets is very different from the bulk-derived one and that the difference in energy is quite large. Our results are of general interest as they should be applicable to all stoichiometries of MgB_x as well as to other metal borides.

II. METHODS

We calculate ground-state properties using density-functional theory with the local-density approximation, plane-wave basis, and norm-conserving pseudopotentials.[38–44] The B pseudopotential has cutoff radii $(r_c^s, r_c^p, r_c^d)=(1.7, 2.1, 1.7)a_0$. For Mg, we use nonlinear core corrections[45] and $(r_c^s, r_c^p, r_c^d)=(2.1, 2.5, 2.5)a_0$. We expand wave functions with an energy cutoff 32 Ry. K-point sam-

pling with a Gaussian smearing width of 0.5 eV converges total energies to better than 1 meV/atom. Our supercells contain 2D sheets extended in xy plane with periodic copies along z direction separated by 7.4 and 15.9 Å for pure boron and MgB_2, respectively. We relax all structures until atomic forces are below 1 meV/Å and stresses are below 50 MPa. We generate maximally localized Wannier functions (MLWFs) using standard algorithms.[46–48]

III. SELF-DOPING IN BORON NANOSTRUCTURES

A. In-plane and out-of-plane states

Our naming system for pure 2D boron sheets involves using a letter followed by the η value.[16] In brief, η is the fraction of atoms removed from a triangular sheet that yields a desired sheet. Thus T(0) is flat triangular, H(1/3) is hexagonal (i.e., graphitic), and A(1/9) is the most stable α sheet.[16,17]

Previously, we discovered that A(1/9) is most stable due to the optimal filling of σ bonds: electrons fill all in-plane bonding σ states while leaving all in-plane antibonding σ^* states empty, and any remaining electrons partially fill out-of-plane π states.[16] The fact that σ bonds are stronger than π bonds explains why best structures are determined by optimal filling of the in-plane manifold.

Following this philosophy, we count the number of in-plane and out-of-plane states for many boron sheets to identify trends. We begin with a large M-atom T(0) sheet and gradually remove atoms: each removal leaves behind a hexagonal hole. For each structure obtained, we calculate the densities of states (DOS) projected onto in-plane and out-of-plane states; mathematically, this means projection onto even and odd parity states with respect to reflection in the sheet plane. We identify the separation energy E_{sep} of in-plane bonding σ and antibonding σ^* states as the energy where the in-plane DOS has a zero (we have checked the validity of this criterion in a few cases by manually plotting wave functions and checking their character in detail). By integrating the in-plane DOS $D_\sigma(\epsilon)$ and out-of-plane DOS $D_\pi(\epsilon)$, we calculate (i) N_σ—the number of in-plane σ bonding states with energy below E_{sep}

$$N_\sigma = \int_{-\infty}^{E_{sep}} d\epsilon D_\sigma(\epsilon), \tag{1}$$

and (ii) N_π—the number of out-of-plane π states with energy below E_{sep}

$$N_\pi = \int_{-\infty}^{E_{sep}} d\epsilon D_\pi(\epsilon). \tag{2}$$

The number of electrons is given by integrating the total DOS up to the Fermi energy E_F,

$$N_e = 2\int_{-\infty}^{E_F} d\epsilon [D_\sigma(\epsilon) + D_\pi(\epsilon)] = 3M(1-\eta). \tag{3}$$

where the factor of 2 accounts for spin and the form $3M(1-\eta)$ comes from the fact that each boron atom has three valence electrons and removing atoms from the original T(0) sheet reduces the number of atoms by a proportion of η (which is justified by the definition of η).

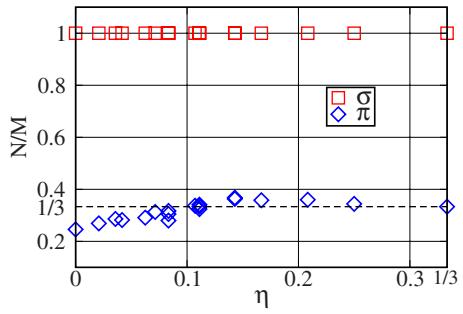

FIG. 1. (Color online) N_σ/M and N_π/M versus η. All data are extracted from *ab initio* plane-wave calculations, red □ for σ and blue ◇ for π states. The horizontal black dashed line shows $N/M=1/3$.

A configuration should be optimal if electrons fill all the in-plane bonding states and leave all the in-plane antibonding states empty with partial occupancy of the π manifold. This simply means $E_F=E_{sep}$ or equivalently

$$2(N_\sigma + N_\pi) = N_e = 3M(1-\eta). \tag{4}$$

Note that Eq. (4) is a constraint on the sheet structure (i.e., the η value) and will hold only for particular sheets that are highly stable.

Based on first-principles calculations, we have discovered that N_σ and N_π are smooth functions of η. Figure 1 shows the behavior of N_σ and N_π versus η for a large collection of boron sheets. As we can see, N_σ/M is precisely unity for all η, and N_π/M always hovers around 1/3. When plugging $N_\sigma=M$ and $N_\pi=M/3$ into Eq. (4), we find the simpler relation

$$2(M + M/3) = 3M(1-\eta). \tag{5}$$

The solution to this equation is $\eta=1/9$ which is precisely the η value for the most stable A(1/9) or α sheet.

The results shown in Fig. 1 are surprising: the number of in-plane bonds remains constant even as we add or remove boron atoms from the boron sheet. Since the interatomic distances are essentially fixed when η changes,[16] adding or removing atoms directly changes the areal density of boron atoms. Naively, we would have expected a higher areal density of atoms to result in a higher density of bonding states. We discuss the reason for this behavior next.

B. Chemical bonding from maximally localized Wannier functions

By investigating the chemical bonding in 2D boron sheets using MLWFs, we can explain the surprising results on constant number of bonds. We consider the evolution of MLWFs when boron sheets change from hexagonal to triangular. For example, Fig. 2(a) shows how a six-atom unit cell of H(1/3) evolves under addition of boron atoms into mixed phase D(2/9), A(1/9), and finally T(0). As per Fig. 1 and detailed analysis of the band structures, all four sheets are found to have nine σ bonding bands. For each sheet, we calculate

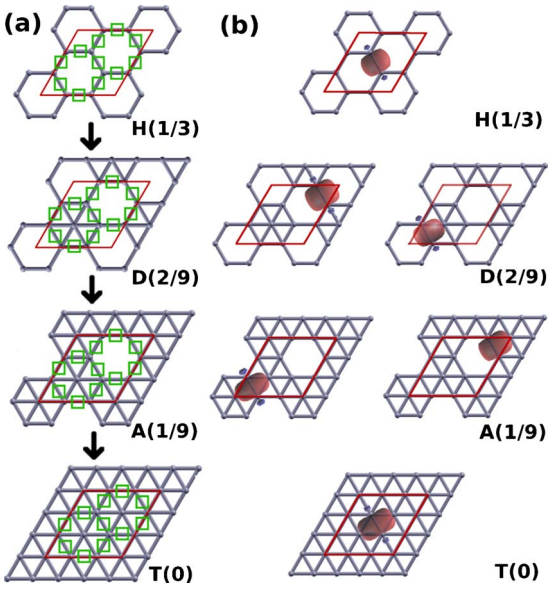

FIG. 2. (Color online) (a) Evolution of boron sheets from H(1/3) to D(2/9), A(1/9), and finally T(0): green "□" mark the centers of σ MLWFs. (b) Isosurface contour plots of representative σ MLWFs for H(1/3), D(2/9), A(1/9), and T(0), respectively: red for positive, blue for negative values; other σ MLWFs are obtained by symmetry. Red solid lines show unit cells.

MLWFs for the lowest 12 bands and obtain nine in-plane (σ) and three out-of-plane (π) MLWFs. We reproduce the nine σ bonding bands in each case by imposing an inner window.[47]

For in-plane states, each sheet has one or two unique types of σ MLWFs due to symmetry (the others are obtained by symmetry operations). We show representative σ MLWFs for each sheet in Fig. 2(b). Sheet H(1/3) has nine identical MLWFs localized in the middle of two adjacent atoms, i.e., two-center bonding. At the other extreme, sheet T(0) is three-center bonded,[16] and we find that it can be described using two different sets of MLWFs: (i) triangular-shaped σ MLWFs centered in the centers of triangles indicating explicitly three-center bonding as shown in Fig. 3(a), or (ii) σ MLWFs shown in Figs. 2(b) and 3(b) which are centered between

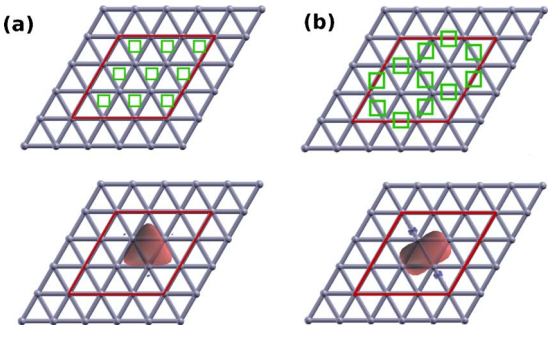

FIG. 3. (Color online) Centers (marked by green □) and isosurface contour plot (red for positive and blue for negative values) of two sets of σ MLWFs for T(0) boron sheet: (a) triangular shaped, (b) rectangular shaped. These σ MLWFs are even with respect to reflection in the plane of the boron sheets. Red solid lines show the unit cells.

adjacent atoms and symmetrically spread to triangles on both sides. These two sets of MLWFs span the same subspace, generate identical band structures, and thus describe the same physics of three-center bonding. We use group (ii) because it shows the most consistent evolution with η below. The two intermediate sheets D(2/9) and A(1/9) each have two types of σ MLWFs. For D(2/9), the first type is similar to that of H(1/3) as it is centered between a B-B pair in a hexagonal environment while the other is asymmetric and spreads toward the neighboring triangular region, i.e., mixing of two- and three-center character. For A(1/9), the first type is in a triangular environment and resembles that of T(0) while the other is asymmetric in the same manner as D(2/9).

After looking at the figures, the main observation is that despite large changes in sheet structure and atomic areal density, the same number of σ MLWFs are basically centered at the same sites as in H(1/3) while showing minor shifts in some cases. Thus, during the evolution of the sheet from hexagonal to triangular, the basic in-plane bonding pattern and number of bonds of the hexagonal system is retained with some minor perturbations in shape and position. (We have checked that these results are general and not restricted to the sheets discussed here.)

Turning to out-of-plane states, due to symmetry, the three π MLWFs of a given sheet are identical and can be transformed into each other by simple translation and rotation. We show the representative π MLWFs for each sheet in Fig. 4(a). For H(1/3), two sets of π MLWFs can be obtained depending on the choice of initial guess. These two sets of π MLWFs reproduce the same band structure, span the same subspace, and thus describe the same physics. We label them H(1/3)(i) and H(1/3)(ii) in Fig. 4. The π MLWF in H(1/3)(i) is peanutlike and centered in the middle of the B-B line connecting two boron atoms. On the other hand, H(1/3)(ii) is centered on a boron atom and spreads to its three nearest neighbors. For the other extreme, the sheet T(0), π MLWF is centered on a boron atom and spreads to its six nearest neighbors. The π MLWFs of the two mixed-phase sheets [D(2/9) and A(1/9)] differ from each other. For D(2/9), the MLWF is centered on a boron atom and spreads to four nearest neighbors, while for A(1/9), the MLWF is centered in the middle of a B-B pair and spreads to these two boron atoms and two other boron atoms in the two neighboring triangular regions. When looking at the centers of these π MLWFs, as shown in Fig. 4(b), we discover that π MLWFs evolve with the structures of boron sheets in almost the same way as σ MLWFs. As we can see, sheets D(2/9) and T(0) have π MLWFs centered on the same sites as H(1/3)(ii), which are on every other atoms of the H(1/3)'s lattice. On the other hand, sheet A(1/9) has π MLWFs centered on the same sites as H(1/3)(i), which are on every other B-B bonds of the H(1/3)'s lattice. Although we do not have all sheets sharing the same π MLWF centers like what we have for σ MLWFs, we do have the bonding patterns of three sheets, D(2/9), A(1/9) and T(0), originating from the same parent system H(1/3). In details, the π manifolds of D(2/9) and T(0) originate from H(1/3)(ii), and that of A(1/9) originates from H(1/3)(i).

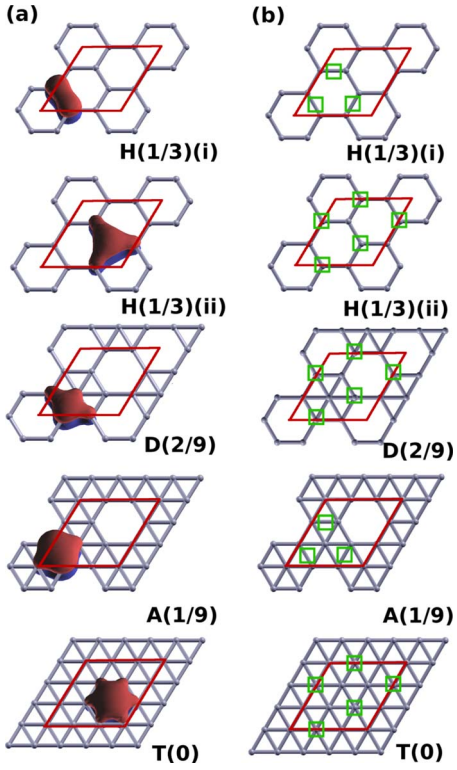

FIG. 4. (Color online) (a) Isosurface contour plots of representative π MLWFs for H(1/3), D(2/9), A(1/9), and T(0), respectively: red for positive, blue for negative values; other π MLWFs are obtained by symmetry. These π MLWFs are odd with respect to reflection in the plane of the boron sheets. (b) Centers of π MLWFs shown by green □. Red solid lines show the unit cells.

C. Self-doping and a general design rule

The above analysis leads to the following picture for boron sheets: adding a boron atom to fill a hexagonal hole in a 2D boron sheet does not change the number of bonding states but simply causes the three valence electrons of the added atom to be released into the lattice. In other words, adding a boron is equivalent to doping the original boron system with three more valence electrons. We call this unusual situation self-doping. Since 2D boron sheets are precursors of atomically thin boron nanotubes and fullerenes, self-doping is generally useful and applicable. For example, self-doping provides a general design rule for stable boron nanostructures. If we start with a stable graphene-derived carbon nanostructure with Z atoms containing many hexagon motifs, we could contemplate replacing all carbon with boron. However, to make a stable structure, we would need to add boron atoms since boron has only three valence electrons compared to carbon's four, and we need an extra electron per atom (Z extra electrons in total) to fill the bonding states. The solution is simple: if we fill the hexagon center sites with additional $Z/3$ boron atoms, they will each donate three electrons (exactly Z electrons in total) without changing the bonding states, making the structure isoelectronic to the original carbon system, and thus stabilize the final boron structure.

This design rule explains the fact that the A(1/9) sheet and the stable B_{80} fullerene[19] can be derived from graphene and the C_{60} fullerene by filling hexagonal holes with extra atoms. Moreover, it explains why stable $B_{80+8k}(k \geq 0, k \neq 1)$ fullerenes can be built from the corresponding $C_{60+6k}(k \geq 0, k \neq 1)$ fullerenes.[20] Finally, our design rule also sheds light on the recently discovered families of stable boron fullerenes.[21,22]

IV. METAL BORIDE NANOSTRUCTURES

A. Self-doping applied in metal borides

Beyond pure boron nanostructures, self-doping provides a powerful tool for gaining a zeroth-order view of metal boride systems. In metal boride structures, we expect that the boron-boron bonding is much stronger than the metal-boron or metal-metal bonding. Furthermore, we expect the metal atoms to donate electrons to the boron subsystem. Therefore, a stable metal boride 2D sheet should have optimally filled boron bonds as a starting point.

Consider a MeB_x system where Me is a metal atom. Assuming that each metal atom donates y electrons to the boron subsystem and does not otherwise perturb the electronic structure, each boron atom now has on average $(3+y/x)$ electrons and the total number of electrons for the boron subsystem is now

$$N_e = (3 + y/x)M(1 - \eta). \tag{6}$$

As discussed in Sec. III A, optimal filling of the boron subsystem means $E_F = E_{sep}$ or equivalently $2(N_\sigma + N_\pi) = N_e$. Since we assume the electronic structure of boron subsystem remains fixed after doping, we still assume that $N_\sigma = M$ and $N_\pi = M/3$. Therefore, to achieve the MeB_x system with optimal stability, the following constraint should be satisfied,

$$2(M + M/3) = (3 + y/x)M(1 - \eta_{optimal}). \tag{7}$$

The solution is

$$\eta_{optimal} = \frac{1 + 3y/x}{9 + 3y/x}. \tag{8}$$

Therefore, if we can estimate the charge transfer y, we estimate the optimal η for any x and thus greatly narrow down the search space for the most stable 2D metal boride structures.

B. Charge transfer

Unfortunately, charge transfer is not easy to calculate precisely because there is no unique way to assign electrons to atoms. One popular way is to calculate Löwdin charges by projecting electronic states to orthogonalized atomic orbitals.[49,50] However, Löwdin orbitals form an incomplete basis with long-ranged tails, and this method may lead to unreasonable charge-transfer results. For instance, in bulk MgB_2, one rational way to explain its stability is that each Mg atom donates all its two valence electrons to the boron honeycomb lattice, making boron lattice isoelectronic to graphene and stabilizing the structure. Following this explanation, which is consistent with our method based on self-doping picture, we expect the charge transfer from Mg to

boron to be essentially complete and close to two electrons per Mg. However, our Löwdin analysis gives only 0.76 e/Mg charge transfer. Therefore, in order to apply self-doping in metal boride systems, a scheme that gives more reasonable charge transfer is necessary.

Here we propose to compute charge transfer by projecting wave functions onto MLWFs: these are an exponentially decaying, maximally localized, orthogonal, and complete basis.[46–48] For Mg-B systems, we found it easy to assign MLWFs to Mg or B atoms by simple visual inspection. For bulk MgB_2, we calculate MLWFs for six lowest bands, obtaining five MLWFs for B which are similar to those of H(1/3), and one MLWF around Mg [see Fig. 5(a)]. Projecting the DOS onto these MLWFs and integrating up to the Fermi energy gives a very reasonable charge transfer of 1.82 e/Mg or approximately Mg^{2+}. Therefore, we believe that the MLWF-based charge transfer gives sensible values for our self-doping method and we use it to calculate charge transfer below.

Again, we would like to emphasize that, formally, charge transfer is an ill-determined quantity depending on details of how it is defined and calculated. However, our main use of the charge transfer will be to make zeroth-order *estimate* of $\eta_{optimal}$ in Eq. (8) in order to describe the basic properties of stable metal borides. For such an application, we believe that as long as the charge transfer can be reasonably defined—such as in our case involving a metal atom that is chemically expected to donate electrons to the boron subsystem—the overall approach will be useful.

C. MgB_2 sheets

We illustrate this approach based on self-doping for 2D atomically thin MgB_2 sheets. (Enlarging the project to other MgB_x stoichiometries is a future project.) Figure 5 shows three MgB_2 sheets: Fig. 5(b) is the bulk-derived sheet structure with Mg on H(1/3), Fig. 5(c) is based on a G(3/10) boron sheet, and Fig. 5(d) is built from an E(1/5) boron sheet. These MgB_2 sheets are illustrated in Figs. 7(e)–7(g). The MLWF charge transfers are 1.37, 1.05, and 0.62 e/Mg, respectively, which are quite different from and clearly smaller than 1.82 e/Mg (the bulk MgB_2 value). This already suggests that the MgB_2 sheet structure derived from bulk will not be most stable.

Furthermore, we notice that the charge transfers of three MgB_2 sheets are different from each other. Hence, the charge transfer y and the optimal η are interdependent quantities: rigorously, Eq. (8) should be solved self-consistently in y and x. However, since the method is approximate and we wish to present a zeroth-order view, we note that, very crudely, y hovers around unity. Using a guess of $y=1$ in Eq. (8) yields $\eta_{optimal}=5/21$ which suggests that Mg placed on $\eta\approx 1/4$ boron sheets should create the most stable MgB_2 sheets.

To test this method, we construct many MgB_2 sheets by putting Mg on different boron sheets with a range of η. Figure 6 shows the energies of the best MgB_2 sheets we found for each η and Fig. 7 shows their atomic geometries. The optimal MgB_2 sheet we have found, shown in Fig. 7(a), occurs at $\eta=1/4$ and is obtained by doping Mg on an F(1/4)

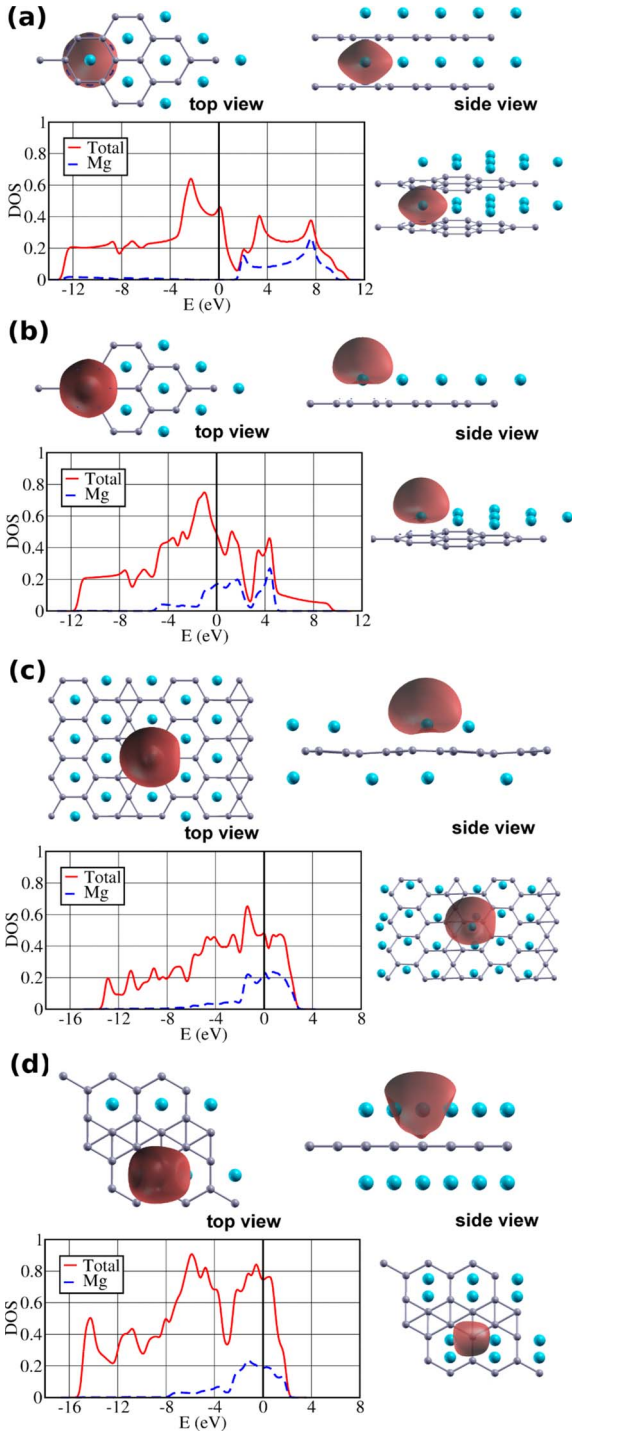

FIG. 5. (Color online) Isosurface contour plots of MLWFs associated with Mg (top, side and best-angle view, red for positive and blue for negative values), total DOS (red solid lines) and partial DOS on Mg (blue dashed lines) for (a) MgB_2 bulk, (b) MgB_2 sheet derived from bulk with Mg on the H(1/3) sheet, (c) MgB_2 sheet from a G(3/10) boron sheet, and (d) MgB_2 sheet based on an E(1/5) boron sheet. The charge transfers from Mg to B are (a) 1.82, (b) 1.37, (c) 1.05, and (d) 0.62 e/Mg. For the MgB_2 sheet in (c), there are two types of MLWFs associated with Mg: we only show one of them while the other is very similar to the one in (d). Small gray balls are boron and large blue green balls are Mg. Black solid lines are the Fermi levels.

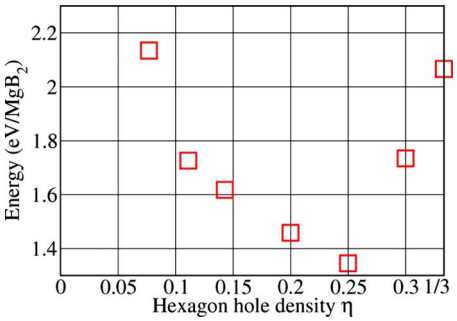

FIG. 6. (Color online) Red squares show the energies (measured relative to bulk MgB_2) per formula unit of the most stable MgB_2 sheets at each η versus η. The optimal MgB_2 sheet structure occurs at $\eta=1/4$ [whose image is shown in Fig. 7(a)]. The point at $\eta=1/3$ corresponds to the bulk-derived sheet structure.

boron sheet. This particular MgB_2 sheet is 0.72 eV/MgB_2 more stable than the bulk-derived one ($\eta=1/3$), which is a significant energy difference. We believe that this sheet is a better precursor for MgB_2 nanotubes.

During the above search process, we found the following rules of thumb to hold when generating stable MgB_2 sheets. While we are not able to present a proof, we believe they should be generally applicable to other stoichiometries. In order to make the lowest-energy structure, one should: (a) to whatever extent possible, put Mg on the hexagon sites (above or below the boron sheet), (b) fill both sites above

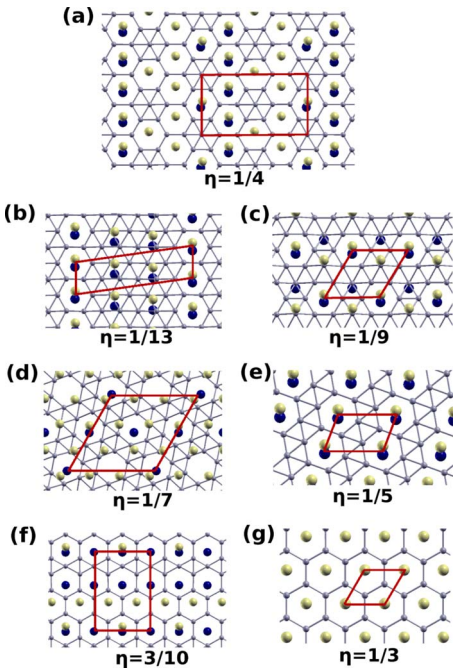

FIG. 7. (Color online) The most stable MgB_2 sheets for (a) $\eta=1/4$, (b) $\eta=1/13$, (c) $\eta=1/9$, (d) $\eta=1/7$, (e) $\eta=1/5$, (f) $\eta=3/10$, and (g) $\eta=1/3$. The structure in (a) is the best MgB_2 sheet in our library. We display top views that are rotated slightly around the horizontal (x) axis. Small gray balls are B, large light yellow balls are Mg lying above the boron plane, and large dark blue balls are Mg lying below the boron plane. Red solid lines show the primitive cells.

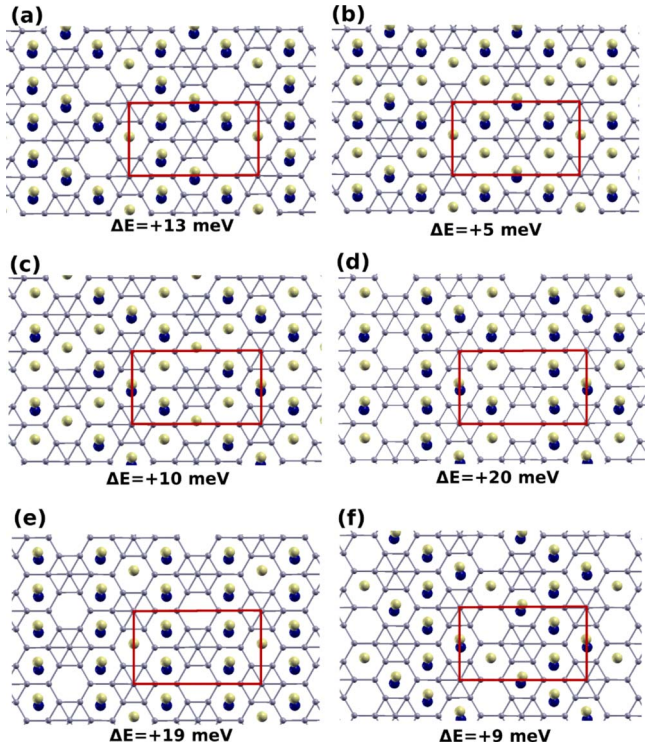

FIG. 8. (Color online) MgB_2 sheet structures derived from the same F(1/4) boron sheet sublattice but with different Mg distributions from the optimal MgB_2 sheet shown in Fig. 7(a). These sheets are all less stable than the optimal structure. The energy differences, in meV per formula unit, are shown below each structure. We display top views that are rotated slightly around the horizontal (x) axis. Small gray balls are B, large light yellow balls are Mg lying above the boron plane, and large dark blue balls are Mg lying below the boron plane. Red solid lines show the primitive cells.

and below the hexagon if needed, and (c) put the any remaining Mg in the triangular regions. Only a very small number of our most stable MgB_2 sheets do not obey these rules, e.g., the sheet in Fig. 7(d).

To exemplify these rules, for the fixed boron sublattice of sheet F(1/4), we constructed a few variants of the optimal MgB_2 sheet [Fig. 7(a)] where only the distribution of Mg atoms among hexagon sites was varied. These MgB_2 sheets, which are shown in Fig. 8, are all less stable than the optimal one but only by at most 20 meV/MgB_2. Thus while a search over possible Mg arrangements is needed to find the true ground state, this part of the search does not contribute greatly to the total energy as long as all Mg atoms occupy hexagon sites. In summary, the combination of the optimal η from Eq. (8) and the above rules for the best Mg placement greatly narrows down the search space for optimal metal boride nanostructures.

V. CONCLUSIONS AND OUTLOOK

In conclusion, we present a self-doping mechanism in boron nanostructures based on a clear analysis of the chemical bonding in boron sheets using MLWFs. We propose a general design rule for boron nanostructures based on self-

doping which explains many stable boron structures discovered in other work. Moreover, self-doping provides a tool for studying metal-doped boron nanosystems and we use it to discover a stable atomically thin MgB_2 sheet. The method is general, applicable to other metal borides, and should help in designing and understanding the properties of metal-doped boride nanotubes and other nanostructures.

We close by noting two points concerning our results. First, this work has focused on the properties and stability of isolated atomically thin 2D boron and metal boride nanostructures (and by extension isolated nanotubes made of such sheets). A subject of present interest and for future investigation involves the importance of bundling effects when the nanostructures are brought in close proximity. Stabilizing effects of bundling have been already demonstrated for AlB_2 and MgB_2 nanotubes built from 2D sheets derived from AlB_2 and MgB_2 bulk structures.[24,32] How the metal boride structures we propose here are stabilized or modified by bundling is an interesting open question.

Second, our focus has been on finding thermodynamic ground-state structures for pure boron and metal boride nanostructures. Other pure boron nanostructures (such as those built from the triangular sheet[12–15]) or metal doped nanostructures (such as those built from the bulk MgB_2 derived 2D sheet[23,29–32]), while not thermodynamic ground states, are mechanically stable (i.e., metastable) and, in principle, might be fabricated during experimental growth via kinetic limitations. Clearly, understanding the growth processes of boron nanostructures is an important topic for future work in terms of seeing whether and how metastable nanostructures might be fabricated, as well as helping realizing a larger variety of boron nanosystems in experiments.

ACKNOWLEDGMENTS

This work was supported primarily by the National Science Foundation under Contract No. DMR-0808665. The Bulldog parallel computer clusters of the Yale High Performance Computing center provided computational resources.

[1] D. Ciuparu, R. F. Klie, Y. Zhu, and L. Pfefferle, J. Phys. Chem. B **108**, 3967 (2004).
[2] B. Kiran, S. Bulusu, H. J. Zhai, S. Yoo, X. C. Zeng, and L. S. Wang, Proc. Natl. Acad. Sci. U.S.A. **102**, 961 (2005).
[3] I. Boustani, Phys. Rev. B **55**, 16426 (1997).
[4] I. Boustani, Surf. Sci. **370**, 355 (1997).
[5] I. Boustani, A. Rubio, and J. A. Alonso, Chem. Phys. Lett. **311**, 21 (1999).
[6] I. Boustani, A. Quandt, and A. Rubio, J. Solid State Chem. **154**, 269 (2000).
[7] S. Chacko, D. G. Kanhere, and I. Boustani, Phys. Rev. B **68**, 035414 (2003).
[8] H.-Jin Zhai, A. N. Alexandrova, K. A. Birch, A. I. Boldyrev, and L.-S. Wang, Angew. Chem., Int. Ed. **42**, 6004 (2003).
[9] H. J. Zhai, B. Kiran, J. L. Li, and L. S. Wang, Nature Mater. **2**, 827 (2003).
[10] H. J. Zhai, L. S. Wang, A. N. Alexandrova, and A. I. Boldyrev, J. Chem. Phys. **117**, 7917 (2002).
[11] A. N. Alexandrova, A. I. Boldyrev, H. J. Zhai, and L. S. Wang, J. Phys. Chem. A **108**, 3509 (2004).
[12] M. H. Evans, J. D. Joannopoulos, and S. T. Pantelides, Phys. Rev. B **72**, 045434 (2005).
[13] J. Kunstmann and A. Quandt, Phys. Rev. B **74**, 035413 (2006).
[14] K. C. Lau and R. Pandey, J. Phys. Chem. C **111**, 2906 (2007).
[15] I. Cabria, M. J. Lopez, and J. A. Alonso, Nanotechnology **17**, 778 (2006).
[16] H. Tang and S. Ismail-Beigi, Phys. Rev. Lett. **99**, 115501 (2007).
[17] X. Yang, Y. Ding, and J. Ni, Phys. Rev. B **77**, 041402(R) (2008).
[18] A. K. Singh, A. Sadrzadeh, and B. I. Yakobson, Nano Lett. **8**, 1314 (2008).
[19] N. Gonzalez Szwacki, A. Sadrzadeh, and B. I. Yakobson, Phys. Rev. Lett. **98**, 166804 (2007).
[20] Q.-B. Yan, X.-L. Sheng, Q.-R. Zheng, L.-Z. Zhang, and G. Su, Phys. Rev. B **78**, 201401(R) (2008).
[21] R. R. Zope, EPL **85**, 68005 (2009).
[22] R. R. Zope, T. Baruah, K. C. Lau, A. Y. Liu, M. R. Pederson, and B. I. Dunlap, Phys. Rev. B **79**, 161403(R) (2009).
[23] L. A. Chernozatonskii, JETP Lett. **74**, 335 (2001).
[24] A. Quandt, A. Y. Liu, and I. Boustani, Phys. Rev. B **64**, 125422 (2001).
[25] P. Zhang and V. H. Crespi, Phys. Rev. Lett. **89**, 056403 (2002).
[26] M. Kociak, A. Y. Kasumov, S. Guéron, B. Reulet, I. I. Khodos, Y. B. Gorbatov, V. T. Volkov, L. Vaccarini, and H. Bouchiat, Phys. Rev. Lett. **86**, 2416 (2001).
[27] I. Takesue, J. Haruyama, N. Kobayashi, S. Chiashi, S. Maruyama, T. Sugai, and H. Shinohara, Phys. Rev. Lett. **96**, 057001 (2006).
[28] J. Nagamatsu, N. Nakagawa, T. Muranaka, Y. Zenitani, and J. Akimitsu, Nature (London) **410**, 63 (2001).
[29] S. Saito, S. G. Louie, and M. L. Cohen, J. Phys. Soc. Jpn. **76**, 043707 (2007).
[30] V. Pokropivny, Int. J. Nanotechnol. **1**, 170 (2004).
[31] V. V. Ivanovskaya, A. N. Enjashin, A. A. Sofronov, Y. N. Makurin, N. I. Medvedeva, and A. L. Ivanovskii, J. Mol. Struct.: THEOCHEM **625**, 9 (2003).
[32] D. L. V. K. Prasad and E. D. Jemmis, J. Mol. Struct.: THEOCHEM **771**, 111 (2006).
[33] Y. Zhu, F. Liu, W. Ding, X. Guo, and Y. Chen, Angew. Chem., Int. Ed. **45**, 7211 (2006).
[34] Y. Zhu, X. Guo, M. Mo, X. Guo, W. Ding, and Y. Chen, Nanotechnology **19**, 405602 (2008).
[35] S. Guerini and P. Piquini, Microelectron. J. **34**, 495 (2003).
[36] S. Meng, E. Kaxiras, and Z. Zhang, Nano Lett. **7**, 663 (2007).
[37] Y. Zhao, M. T. Lusk, A. C. Dilon, M. J. Heben, and S. B. Zhang, Nano Lett. **8**, 157 (2008).
[38] P. Hohenberg and W. Kohn, Phys. Rev. **136**, B864 (1964).
[39] W. Kohn and L. J. Sham, Phys. Rev. **140**, A1133 (1965).
[40] J. P. Perdew and A. Zunger, Phys. Rev. B **23**, 5048 (1981).
[41] M. C. Payne, M. P. Teter, D. C. Allan, T. A. Arias, and J. D. Joannopoulos, Rev. Mod. Phys. **64**, 1045 (1992).

[42] N. Troullier and J. L. Martins, Phys. Rev. B **43**, 1993 (1991).
[43] PARATEC (PARAllel Total Energy Code) is a plane-wave pseudopotential program for parallel computations, http://www.nersc.gov/projects/paratec/
[44] PWscf (Plane-Wave Self-Consistent Field) is a computer code for electronic-structure calculations using pseudopotentials, http://www.pwscf.org/
[45] S. G. Louie, S. Froyen, and M. L. Cohen, Phys. Rev. B **26**, 1738 (1982).
[46] N. Marzari and D. Vanderbilt, Phys. Rev. B **56**, 12847 (1997).
[47] I. Souza, N. Marzari, and D. Vanderbilt, Phys. Rev. B **65**, 035109 (2001).
[48] A. A. Mostofi, J. R. Yates, Y.-S. Lee, I. Souza, D. Vanderbilt, and N. Marzari, Comput. Phys. Commun. **178**, 685 (2008).
[49] P.-O. Löwdin, J. Chem. Phys. **18**, 365 (1950).
[50] D. Sanchez-Portal, E. Artacho, and J. M. Soler, Solid State Commun. **95**, 685 (1995).